



DOI: 10.22144/ctu.jen.2023.014

## Synthesis and application of $\text{Fe}_3\text{O}_4/\text{GO}/\text{PVP}$ composite material for methylene blue adsorption

Luong Huynh Vu Thanh<sup>1,2\*</sup>, Nguyen Thi Nhu Y<sup>3\*</sup>, Nguyen Van Kiet<sup>3</sup>, Ngo Truong Ngoc Mai<sup>2</sup>, Nguyen Nhu Ngoc<sup>2</sup>, and Ly Phuong Thao<sup>2</sup>

<sup>1</sup>Applied Chemical Engineering Lab, College of Engineering Technology, Can Tho University, Viet Nam

<sup>2</sup>Department of Chemical Engineering, College of Engineering Technology, Can Tho University, Viet Nam

<sup>3</sup>Can Tho University of Technology, Viet Nam

\*Correspondence: Luong Huynh Vu Thanh (email: lhvthanh@ctu.edu.vn);

Nguyen Thi Nhu Y (email: ntny@ctu.edu.vn)

### Article info.

Received 14 Jun 2022

Revised 30 Sep 2022

Accepted 11 Mar 2023

### Keywords

$\text{Fe}_3\text{O}_4$ , graphene oxide, methyl blue removal, magnetic adsorbent, PVP

### ABSTRACT

In this study,  $\text{Fe}_3\text{O}_4/\text{GO}/\text{PVP}$  (FGP) was successfully synthesized and efficiently applied for absorbing methylene blue. First, GO was synthesized by Hummer's method from waste home-batteries. The chemical coprecipitation method was used to fabricate  $\text{Fe}_3\text{O}_4/\text{GO}$  from a mixture solution of GO,  $\text{Fe}_3^+$ ,  $\text{Fe}_2^+$ . Polyvinylpyrrolidone PVP was selected to functionalize  $\text{Fe}_3\text{O}_4/\text{GO}$  and form  $\text{Fe}_3\text{O}_4/\text{GO}/\text{PVP}$  for improving dispersibility purpose in aqueous solution. The obtained  $\text{Fe}_3\text{O}_4/\text{GO}/\text{PVP}$  was characterized by XRD, FT-IR, BET, FE-SEM, UV-Vis techniques. Moreover, the effecting factors as pH, time adsorption, initial concentration of methylene blue were conducted. Adsorption isotherm models were also identified. The results showed that specific surface area of FGP-3 was  $70.0 \text{ m}^2.\text{g}^{-1}$ , the Freundlich isotherm model was suitable and the Dubinin - Radushkevich isotherm model showed that the process was physical adsorption. The maximum capacity ( $q_{\text{max}}$ ) was  $30.4 \text{ mg.g}^{-1}$ . These findings prove  $\text{Fe}_3\text{O}_4/\text{GO}/\text{PVP}$  as an inexpensive and efficient adsorbent for removal of cationic dyes.

## 1. INTRODUCTION

Various dyes have been used in the production processes of the textile dyeing and printing (Munoz et al., 2018). These organic dyes are non-degradable, mutagenic, toxic and carcinogenic to humans (Wang et al., 2015; Xiao et al., 2016). Among them, methylene blue (MB) is commonly used to dye wool, cotton and silk which causes various complications such as redness and itching, irritation of skin, throat, mouth, oesophagus, stomach gastrointestinal tract issues, nausea, vomiting, diarrhoea, dizziness, headache, and fever (Stawinski et al., 2017; Munoz et al., 2018).

Therefore, it is necessary to find simple, and efficient methods to treat dye wastewater.

Many technologies have been applied to treat organic wastewater such as biological, chemical or physical methods. Among these techniques, adsorption is one of the most favoured methods because of its low cost, ease of operation, lower energy consumption, simple setup, high efficiency and non-toxicity (Saini et al., 2017). One of the major challenges is identifying novel adsorbents that successfully remove some pollutants from wastewater sources, improving the adsorption efficiency compared to traditional materials such as

biological, inorganic and activated carbon materials (Zhang et al., 2017; Wei et al., 2018).

Hundreds of millions of batteries are used in electronic devices annually. To date, tons of toxic materials from these batteries are released globally, since collecting and recycling of waste batteries has been limited. Therefore, utilization of used-battery sources as adsorbent material will contribute to reducing pollution and protecting public health.

Graphene oxide (GO) is an attractive material for heavy metal ion removal and pigment adsorption because of its two-dimensional structure and high specific surface area ( $2630 \text{ m}^2 \cdot \text{g}^{-1}$ ). However, it is difficult to recover GO after using for adsorption applications (Dreyer et al., 2010; Morimoto et al., 2016; Brisebois et al., 2020).

Iron oxide ( $\text{Fe}_3\text{O}_4$ ) has increasingly been investigated because of its unique properties such as magnetism, biocompatibility, low toxicity and catalytic ability.  $\text{Fe}_3\text{O}_4$  with magnetism can improve the recovery of GO through the external magnetic field after adsorption (Cui et al., 2015).

Polyvinylpyrrolidone (PVP) is a non-conductive, soluble and non-toxic polymer. PVP contains a large number of functional groups such as C=O and C-N providing multiple colorant adsorption sites. In this study, PVP was used to stabilize the surface and improve dispersibility of  $\text{Fe}_3\text{O}_4/\text{GO}$  nanocomposites. The obtained  $\text{Fe}_3\text{O}_4/\text{GO}/\text{PVP}$  nanocomposites are applied as a cheap and efficient adsorbent for organic effluent treatment, specifically Methyl Blue (MB).

## 2. MATERIALS AND METHOD

### 2.1. Chemicals and Materials

Graphite was prepared from used batteries. Potassium permanganate (99%, Vietnam), Sulfuric acid (98%, China), Sodium nitrate (99%, China), Hydrogen peroxide (30%, China), Ethanol (96%, Vietnam), Iron (II) chloride tetrahydrate (99%, China), Iron (III) chloride hexahydrate (99%, China), ammonium hydroxide (China), Hydrochloric acid (36%, China), Sodium hydroxide (96%, China), Methylene Blue (98.5%, China) and Poly vinyl pyrrolidone (11.5%, Sigma Aldrich).

### 2.2. Preparation of $\text{Fe}_3\text{O}_4/\text{GO}/\text{PVP}$

GO was synthesized by the Hummer method as outlined in the literature (Hummer et al., 1958), whereby the ratios of Graphite: $\text{NaNO}_3$ : $\text{H}_2\text{SO}_4$  (g/g/g) were 2:2.5:138 (GO-2) and 2.5:2.5:138 (GO-

2.5) for comparison. Next,  $\text{Fe}_3\text{O}_4/\text{GO}$  (FG) was synthesized via the co-precipitation method. Briefly, 0.30 mg GO was dispersed in 150 mL DI water, and sonicated for 30 min, then slowly dropped into salt solution (0.34 g  $\text{FeCl}_3 \cdot 4\text{H}_2\text{O}$ , 0.56 g  $\text{FeCl}_3 \cdot 6\text{H}_2\text{O}$  and 50 mL DI water), continuously stirred for 30 min at  $60^\circ\text{C}$  and aerating  $\text{N}_2$  throughout the process. The  $\text{NH}_4\text{OH}$  23% solution was then added and adjusted to pH 10. The reaction was maintained at  $60^\circ\text{C}$  and continuously stirred for 3 h.  $\text{Fe}_3\text{O}_4/\text{GO}$  products were collected at room temperature and washed by ethanol and DI water. The preparation of  $\text{PVP}/\text{Fe}_3\text{O}_4/\text{GO}$  was followed. In detail, 20 mL each of 1%, 3% and 6% PVP solutions were added in order into every 100 mL  $\text{Fe}_3\text{O}_4/\text{GO}$  to create FGP-1, FGP-3, FGP-6, respectively. The reaction was carried at  $80^\circ\text{C}$ , stirred for 4 h with  $\text{N}_2$  aeration throughout the process. Finally, the obtained  $\text{PVP}/\text{Fe}_3\text{O}_4/\text{GO}$  composites (FGP-1, FGP-3, FGP-6) were collected by magnets.

### 2.3. Characterization

The structural and morphology characterizations of  $\text{PVP}/\text{Fe}_3\text{O}_4/\text{GO}$  were performed by X-ray diffraction analysis (XRD Equinox 5000, Thermo Scientific, France), Fourier transform infrared spectroscopy (FT-IR Nicolet 6700 -Thermo company) and Field emission scanning electron microscope (FE-SEM). Dynamic light scattering (DLS) was used to determine size distribution, specific surface area of absorbing materials was determined by BET method (Brunaure - Emmett - Teller). MB concentration was identified by UV-Vis, adsorption kinetics and type were investigated by experiential calculating and compared to theoretical Langmuir, Freundlich, and Dubinin-Radushkevich models.

### 2.4. Applications of $\text{Fe}_3\text{O}_4/\text{GO}/\text{PVP}$ for Methyl Blue removal

#### 2.4.1. Identifying point of zero charge - PZC

In this experiment, 10 mg of each type of material (FGP-1, FGP-3, FGP-6) was dissolved in 25 mL of KCl 0.1M, pH values were adjusted at certain levels from 3 to 11 by NaOH 0.1M and HCl 0.1M solutions. After shaking for 24 h, pH values were re-identified. Finally, the  $\text{pH}_{\text{PZC}}$  of  $\text{Fe}_3\text{O}_4/\text{GO}/\text{PVP}$  was noted by the plotting line graph method.

#### 2.4.2. Effecting factors to absorbing capacity of FGP adsorbents on methylene blue

To investigate the adsorption capacity of three adsorbent types (FGP-1, FGP-3, FGP-6), the

volume and concentration of MB solutions were fixed at 50 mL and 10 mg.L<sup>-1</sup>, respectively. Every experiment was conducted with 10 mg of each adsorbent type (FGP-1, FGP-3, FGP-6). The solutions were sonicated for 30 seconds, continually stirred in a shaker for 60 min at 100 rpm at room temperature. After separating adsorbents by magnets, solutions was collected.

The MB adsorption process was examined following alternating each variable method to determine the optimal conditions for the whole process. The pH factor was adjusted from 4.5 to 8.5 by NaOH 0.1M and HCl 0.1M solutions, the adsorbent concentration varied from 5 mg.L<sup>-1</sup> to 30 mg.L<sup>-1</sup> in 1 - 24 h and adsorbents mass from 5 - 50 mg. The MB concentration after the adsorption process was determined by UV-Vis measurement after separating sorbents. The equilibrium adsorbed concentration,  $q_e$ , and adsorption efficiency,  $E\%$ , were calculated according to the equation:

$$q_e = \frac{(C_0 - C_e)V}{M} \quad \text{and} \quad E(\%) = \frac{C_0 - C_e}{C_0} \times 100$$

Where  $C_0$  (mmol.L<sup>-1</sup>) is the initial MB concentration,  $C_e$  (mmol.L<sup>-1</sup>) is the equilibrium concentration in solution,  $V$  (L) is the total volume of solution, and  $M$  (g) is the sorbent mass.

### 3. RESULTS AND DISCUSSION

#### 3.1. Characterizations

##### 3.1.1. XRD pattern

The X-ray diffraction patterns of Graphite, GO and FGP-3 are shown in Figure 1. Characteristic diffraction peaks of battery-separated graphite  $2\theta$  at 26.58° corresponding to (111) and several low intensity peaks at 43.76° and 54.18°. The main diffraction peaks of graphite were narrow and sharp, showing an ordered and high crystal structure, which was similar to Lipson' study (1942). In addition, the result showed no metal peaks present in these samples.

Graphite oxidation processes with KMnO<sub>4</sub> and high temperature markedly changed the graphite structure. In both samples, new diffraction peaks of 10.91° and 10.58° appeared in the GO-2 and GO-2.5 samples, respectively. The distances between the layers were 8.102 Å and 8.352 Å for the GO-2 and GO-2.5 samples, respectively. These values were larger than that of pure graphite (3.372 Å).

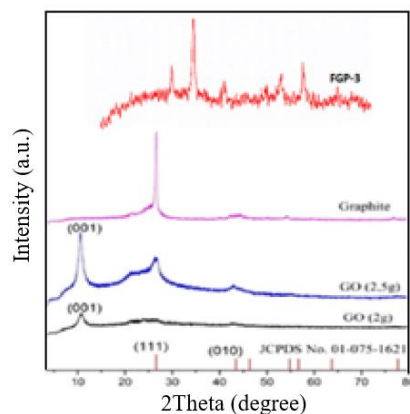


**Figure 1. XRD patterns of Graphite, GO and FGP-3**

The presence of oxygen-containing functional groups in the interlayers facilitates the hydration and delamination process of GO in aqueous environment (Cui et al., 2011; Thema et al., 2013). The distances between GO layers were 0.812 nm, 0.8352 nm compared to pure graphite values of 0.3372 nm. However, the diffraction peaks of the GO-2.5 sample were not sharp, low crystallization and contained graphite peak. The main reason could be that the amount of reducing agent was not enough to remove graphite. Therefore, these peaks had not high crystallinity and the peak of residual graphite remained. In GO-2 sample, a peak at  $2\theta$  of 26.58° did not appear. This showed that the graphite has been completely oxidized and residual metal ions in GO solution disappear.

For FGP-3, the characteristic diffraction peaks shown at  $2\theta$  of 30.01°; 36.1°; 43.7°; 54.08°; 57.6° and 63.06° accordingly with (220), (311), (400), (422), (511) and (440), respectively. These results were consistent with the standard tag (JCPDS No.65-3107) and some previous studies (Chen et al., 2011; Le et al., 2020). The result showed that the crystallinity of Fe<sub>3</sub>O<sub>4</sub> underwent no change after direct coating with GO and surface stabilizing with PVP. The absence of the characteristic diffraction peak of GO ( $2\theta = 10.91^\circ$ ) proved that the GO layers have been completely delaminated by sonication during synthesis process. In addition, there was no crystallization of PVP compared to standard tag. Thus, PVP surfactant could not affect the formation of ferromagnetic particles. However, the diffraction peak of FGP were wider than FG, which showed that PVP could control the size of nanoparticle (Luong et al., 2012). This could be explained the foaming and thermal effects of the ultrasonic waves

on dispersion of the surfactants. The particle size can also be effectively controlled by surfactant under ultrasonic condition (Tural et al., 2009; Feng et al., 2011).

### 3.1.2. FT-IR Infrared Spectrum

The infrared spectrum of the GO sample is shown in Figure 2. In detail, characteristic absorption bands of oxygen-containing functional group at 3684  $\text{cm}^{-1}$  corresponds to the valence vibrations of the O–H bonds. 3024  $\text{cm}^{-1}$  and 2895  $\text{cm}^{-1}$  corresponds to the vibration of the =C–H bond. 2810  $\text{cm}^{-1}$  is the oscillation of the –C–H bond. 1808  $\text{cm}^{-1}$ , 1697  $\text{cm}^{-1}$  corresponds to vibrations of C=O bonds in the aldehyde group, 1554  $\text{cm}^{-1}$ , 429  $\text{cm}^{-1}$  corresponds to vibrations of C=C and 1204  $\text{cm}^{-1}$ , 911  $\text{cm}^{-1}$  are vibrations containing oxygen bonds in the vinyl ether and epoxy groups, respectively (Le, 2019). This again confirms the successful oxidation of graphite to graphene oxide.

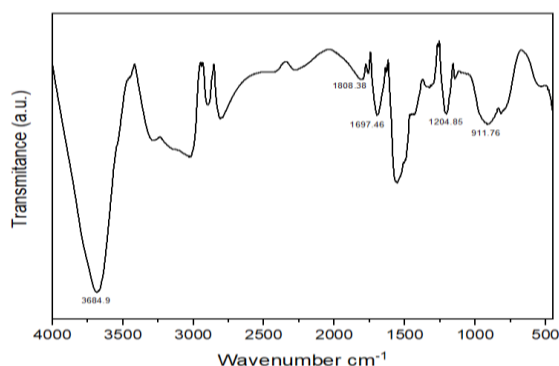


Figure 2. FT-IR of GO

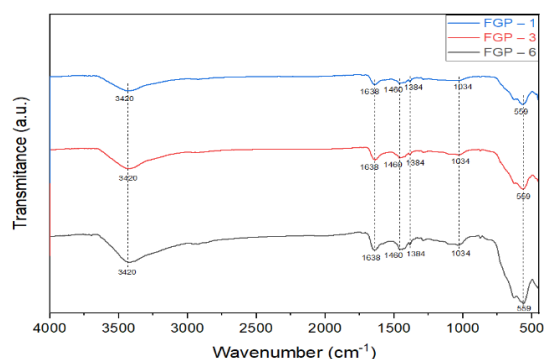


Figure 3. FT-IR of FGP-1, FGP-3 and FGP-6

$\text{Fe}_3\text{O}_4$  particles with peaks at 559  $\text{cm}^{-1}$  of FGP-1, FGP-3 and FGP-6 belong to the stretching vibration region of Fe–O bond, which is characteristic of  $\text{Fe}_3\text{O}_4$  materials (Guan et al., 2010). The absorption bands at 3420  $\text{cm}^{-1}$  are related to the elongation oscillation of –OH. These regions indicate the existence of hydroxyl groups connecting to the surfaces of  $\text{Fe}_3\text{O}_4$  particles in the three samples.

The stretching oscillations of the C=C bond appear at wave numbers of 1638  $\text{cm}^{-1}$  for GO. The appearance of a new peak at wave number of 1460  $\text{cm}^{-1}$  of FGP-1, FGP-3 and FGP-6 samples proved that the – $\text{CH}_2$  group appeared. However, these absorption bands cannot confirm PVP. To confirm that this is the oscillation of the – $\text{CH}_2$  group in PVP, another oscillation of the three samples above at wave number of 1034  $\text{cm}^{-1}$ , which is the oscillation of the C–N bond in the signal region (1200–1025  $\text{cm}^{-1}$ ) (Ibrahim et al., 2013). This proves that there is an interaction between the GO and PVP. Along with that, there is a new peak at wave number of 1384  $\text{cm}^{-1}$  in all three samples, which is also a sign of the appearance of – $\text{CH}_3$  linkage in PVP (Yang et al., 2019). There was almost no difference in oscillation in three samples. Therefore, it is necessary to investigate more factors in the MB adsorption process.

### 3.1.3. Identification of specific surface area

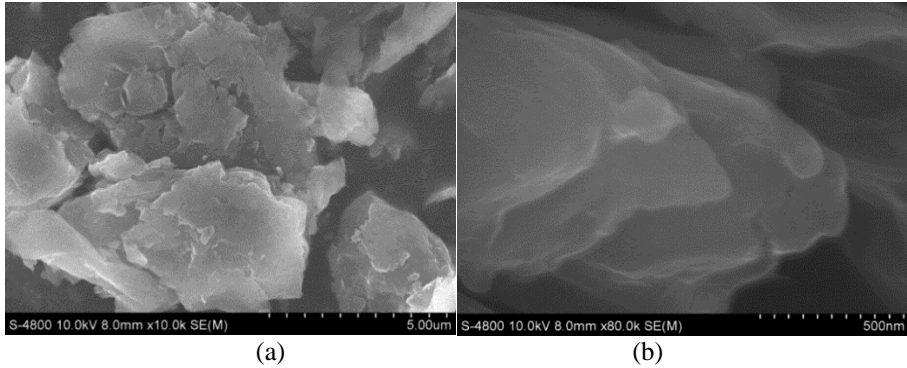
The adsorption and desorption isotherms of GO at 77.3<sup>0</sup>K were identified as type IV according to the IUPAC classification which is typical for layered materials as theoretical definitions. The surface area of GO was 99.1  $\text{m}^2.\text{g}^{-1}$  which was larger than that of FGP-3 (70.0  $\text{m}^2.\text{g}^{-1}$ ) and lower than that of El-Shafai’s study, 253.87  $\text{m}^2.\text{g}^{-1}$  (2020).

Table 1. Structural characteristics of GO and FGP-3

Parameters	Adsorbents	
	GO	FGP-3
Surface area ( $\text{m}^2.\text{g}^{-1}$ ) $S_{\text{BET}}$	99.1	70.0
Capillary diameter (nm) $D_{\text{PORE}}$	2.33	1.20

### 3.1.4. Morphology investigation with FESEM

Morphology of GO with FESEM is shown in Figure 4, highlighting GO with clear separated layers.



**Figure 4. FE-SEM images of GO with magnification of (a) 5.00 µm and (b) 500 nm**

Figure 5 illustrates that the mixture contains both GO and Fe<sub>3</sub>O<sub>4</sub> which are spherical. However, the ferromagnetic particles agglomerate on the GO substrate causing it to be unevenly dense. However, it can be clearly seen that the matrix overall clearly consists of the background (GO) and the filler (Fe<sub>3</sub>O<sub>4</sub>) and Fe<sub>3</sub>O<sub>4</sub> microspheres are anchored on GO, which could effectively prevent the

agglomeration of GO substrate. This result is consistent with the synthesis process of Fe<sub>3</sub>O<sub>4</sub>/GO by co-precipitating method (Qin et al., 2015; Pham et al., 2016). The size distribution chart of the obtained Fe<sub>3</sub>O<sub>4</sub> magnetite particles shows their average size in the range of 14-16 nm with a relatively narrow distribution. This result is almost like the result of Pham (2016).

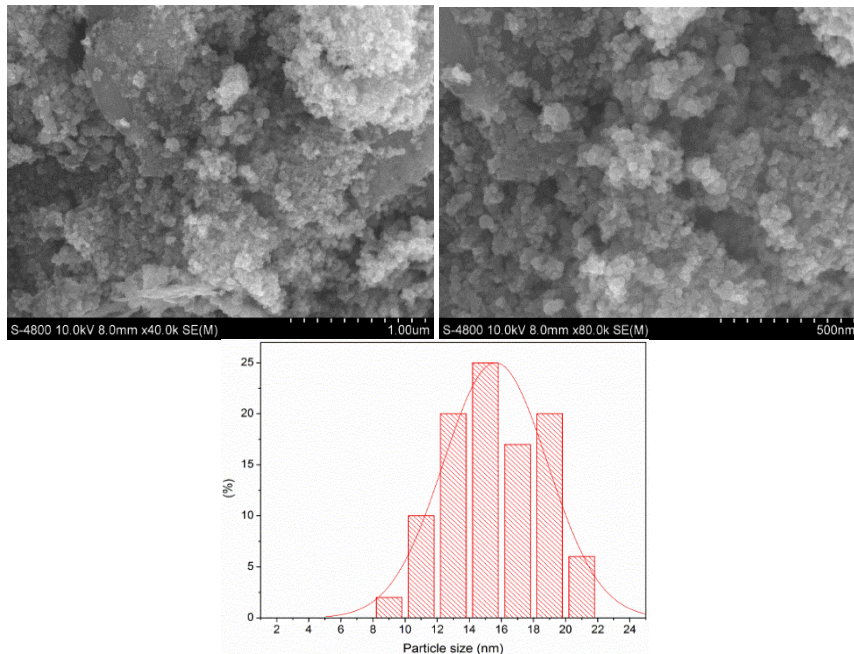


**Figure 5. FE-SEM images with magnification of (a) 1.00 µm, (b) 500 nm and (c) particle size distribution of FGP-3**

### 3.2. Removal of methylene blue using Fe<sub>3</sub>O<sub>4</sub>/GO/PVP

#### 3.2.1. MB adsorption capacity of three adsorbent types

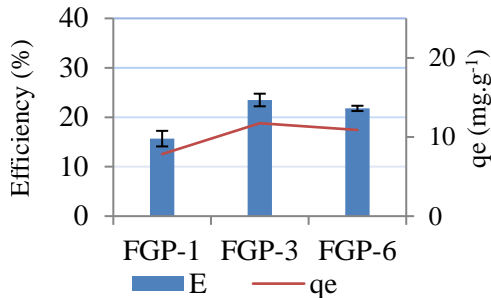


**Figure 6. MB adsorption capacity of three adsorbent types**

Figure 6 showed the adsorption capacity of three adsorbents, namely FGP-1, FGP-3 and FGP-6. The results show that the adsorption capacity of the FGP-3 and FGP-6 were similar with the adsorption efficiency of 23.5% and 21.8%, respectively. For the FGP-1, the recovery efficiency is low, reaching 15.7%. Thus, we selected materials FGP-3 and FGP-6 to conduct the next experiments.

#### 3.2.2. Effect of pH

pH is one of the crucial factors that have the greatest influence on the adsorption capacity of adsorbents in wastewater treatment. The adsorption efficiency depends on the pH of the solution because pH affects not only on the surface charge of the adsorbent but also ionization because of the reacting dye molecule.

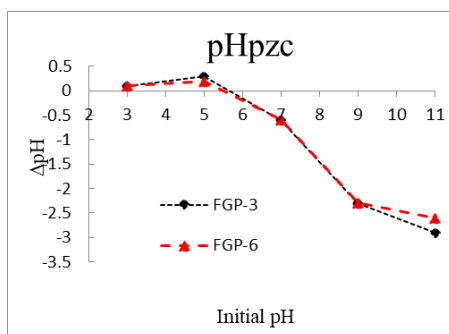


**Figure 7. Identifying pH<sub>pzc</sub>**

Figure 7 shows the surface charge of the two adsorbents types: FGP-3 and FGP-6. The pH<sub>pzc</sub> of the FGP-3 and FGP-6 were 5.6 and 5.5, respectively. From that, it is predicted that these materials will absorb MB well in the base pH range.

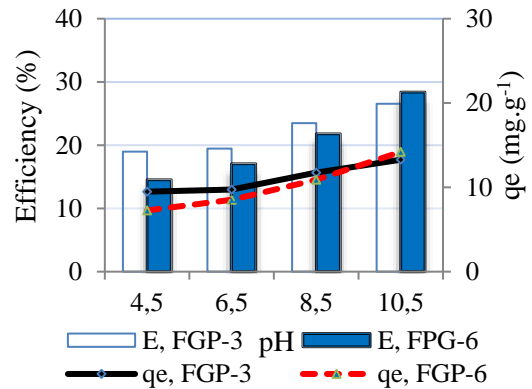


**Figure 8. Effect of pH**

The adsorption capacity of the FGP-3 and FGP-6 increased when the pH increased from 4.5 to 10.5 (Figure 8). Increasing the pH value improved adsorption efficiency and capacity of FGP-3 and FGP-6 on MB. At pH 10.5, the highest efficiency was recorded at 26.6% with FGP-3 and 28.4% with FGP-6, respectively. Thus, pH 10.5 was chosen as the optimal pH condition.

#### 3.2.3. Effect of initial MB concentration on adsorption capacity

Effect of initial MB concentration is presented in Figure 9.

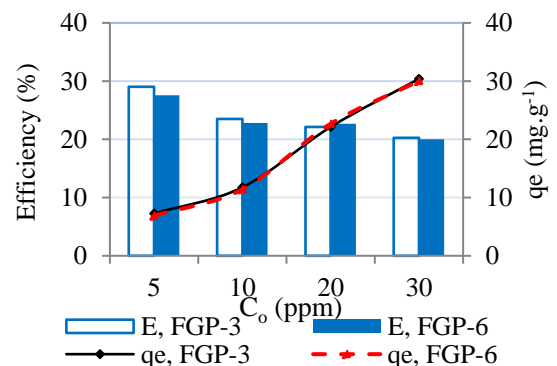


**Figure 9. Effect of initial MB concentration**

Generally, when initial concentration (C<sub>0</sub>) of MB increased, the adsorption capacity of FGP-3 on MB increased while the adsorption efficiency decreased. The initial concentration (C<sub>0</sub>) of MB increased from 5 mg.L<sup>-1</sup> to 30 mg.L<sup>-1</sup>, the efficiency and q<sub>e</sub> changed from 29.0% and 7.26 mg.g<sup>-1</sup> to 20.3% and 30.4 mg.g<sup>-1</sup>. The similar results were seen with FGP-6. This could be explained that when the initial MB concentration was still low (dilute solution), the ions were free to move, the active centres on the surface of adsorbents were not filled with ions, so the

adsorption efficiency additive increased with initial concentration. However, when the initial concentration increased to a certain value, when the active centers were filled with metal ions, the efficiency gradually stabilized and decreased. Therefore, the initial concentration was selected as  $5 \text{ mg}\cdot\text{L}^{-1}$  to investigate the next factors.

### 3.2.4. Effect of time on MB adsorption capacity

The adsorption time is an essential factor that governs the kinetics of the adsorption process and could monitor the usage of adsorbents for practical applications. The effect of time on MB adsorption capacity was investigated between 1 - 24 h as shown in Figure 10.

It can be seen from Figure 10 that the adsorption efficiency of FGP-3 on MB linearly and gradually increased in 1 ÷ 12 h, decreasing gradually in 15 ÷ 24 h. The adsorption capacity reached 67.9% in first 9 h, which was the period when the amount of MB was fastest adsorbed. The initial removal efficiency increased rapidly due to the accessibility of numerous vacant surfactant adsorption sites. Then, over a period of 9 to 12 h, the adsorption efficiency increased from 67.9% to 74.1%. After 12 h, the adsorption efficiency gradually decreased as the amount of surfactant decreased. This could be explained that the sites and molecules have to move farther and deeper into the pores until the adsorption reaches equilibrium. The similarity went for FGP-6 performance rapidly increased from 1 to 9 h and reached equilibrium at 12 h with an adsorption efficiency and capacity of 69.8% and  $17.4 \text{ mg}\cdot\text{g}^{-1}$ , respectively. However, in the same period of 12 h with the FGP-3 material, the adsorption efficiency and capacity were higher than that of the FGP-6 material, 74.1% and  $18.5 \text{ mg}\cdot\text{g}^{-1}$ , respectively. Therefore, FGP-3 was chosen as the optimal adsorbent and the time of 12 h for next experiment.

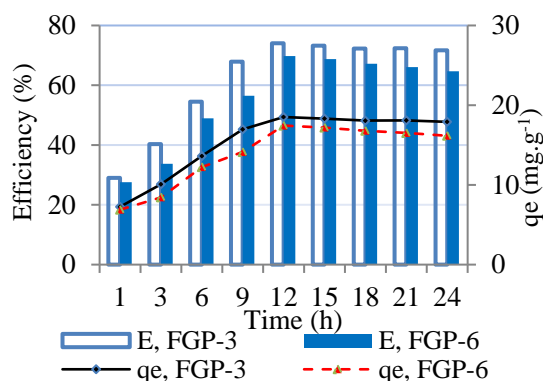


Figure 10. Effect of time adsorption

### 3.2.5. Effect of adsorbent content on MB adsorption capacity

The optimization of the amount of adsorbent for dye adsorption is a necessary parameter to adjust the adsorption capacity of the adsorbent.

Figure 11 shows the relation of FGP-3 mass and MB adsorption efficiency. The adsorption efficiency achieved 54.3% and 74.1% accordingly to 5 mg and 10 mg FGP-3. The highest adsorption efficiency and capacity reached 91.8% and  $22.9 \text{ mg}\cdot\text{g}^{-1}$  with FGP-3 mass of 50 mg. The increase in removal efficiency can be attributed to the enhancement of the overall surface area of the adsorbent and the actively exchangeable adsorption sites. This could be explained by increasing the adsorbent mass will in turn increase the removal efficiency and decrease the adsorption capacity (Mashkour et al., 2020). The effective surface area of the adsorbent per unit mass considerably decreases at its higher concentrations due to interference phenomena such as aggregation or agglomeration. This leads to a decrease in adsorption capacity and many adsorbent sites are still vacant, so the adsorption cannot reach saturation (Iftekhar et al., 2018). Therefore, the optimal FGP-3 mass of 50 mg was selected.

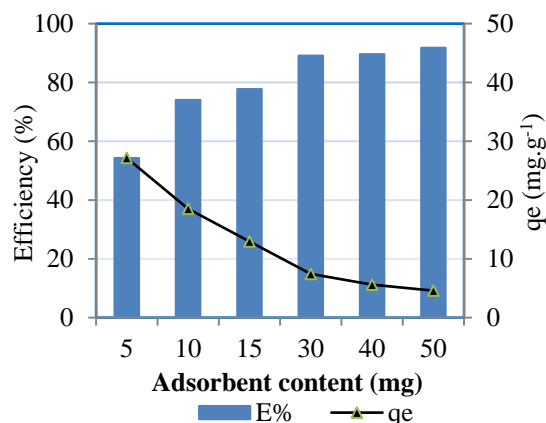


Figure 11. Effect of adsorbent mass

### 3.3. Adsorption kinetics

It is crucial to determine the adsorption kinetics to understand the adsorption mechanism of the adsorbent. In this study, the MB dye adsorption kinetics of FGP-3 followed the hypothetical second-order adsorption model shown in the calculated results (Table 2).

From the parameters of the hypothetical equation in Table 2, it can be seen that the linear regression coefficient  $R^2$  of 0.9925 of the second order was

suitable. The adsorption capacity  $q_e$  of the second-order hypothetical equation approximates the experimental deviation by 1.485% and the reaction rate constant  $K_2 = 0.000406 \text{ g.mg}^{-1}.\text{p}^{-1}$ . This confirmed that the MB adsorption onto FGP-3 followed second-order adsorption kinetics.

Table 2 shows the second-order hypothetical adsorption kinetics with slope  $a = 0.05$ , showing that the adsorption capacity of the material was good.

**Table 2. First and second order hypothetical equation parameters**

	a	b	$q_e \text{ (mg.g}^{-1}\text{)}$	$K_1 \text{ (p}^{-1}\text{)}$	$K_2 \text{ (g.mg}^{-1}.\text{p}^{-1}\text{)}$	$R^2$
1 <sup>st</sup> order Eq	-0.0026	2.1961	8.989	0.0026	–	0.7598
2 <sup>st</sup> order Eq	0.05	6.1622	20.000	–	0.000406	0.9925

**3.4. Isothermal models**

Isotherm adsorption equations are shown in Figure 12. The Freundlich model was suitable with a linear regression coefficient  $R^2$  of 0.9946. The graph showing the relation of  $\log(C_e)$  on  $\log(q_e)$  of MB, Freundlich isotherm constants was 1.31, which was suitable for liquid-solid adsorption system with

theoretical heterogeneity degree between 1 to 10. Besides that, FGP-3 adsorption following the Freundlich adsorption isotherm equation was reversible, the adsorption energy on the surface adsorbents was not uniform, there was mutual interaction between the adsorbed molecules and adsorbents can be multilayer adsorption.

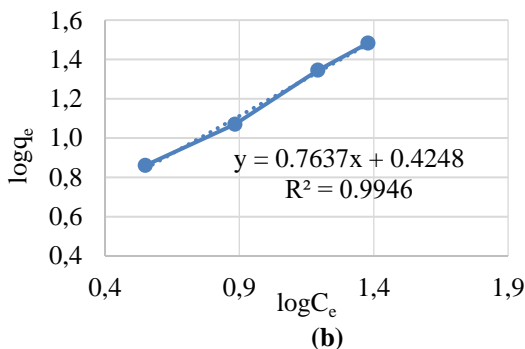
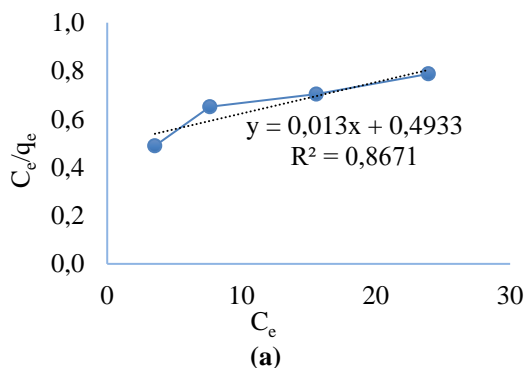


**Figure 12. The isotherm adsorption curves according to (a) Langmuir (b) Freundlich models.**

In order to understand the nature of the MB adsorption process as physical or chemical adsorption, the D-R isothermal adsorption model was applied.

The graph shows that the relation between  $\ln q_e$  and  $\epsilon^2$  (Figure 13) with the coefficient  $R^2$  of 0.805, which show that the  $\beta$  value was 3.2384, the inferring  $E'$  value was 0.393 ( $\text{kJ.mol}^{-1}$ ) can be inferred as  $E' = \frac{1}{\sqrt{2\beta}}$ . With  $E'$  value less than 8  $\text{kJ.mol}^{-1}$ , physical adsorption process was suitable according to theoretical classification .

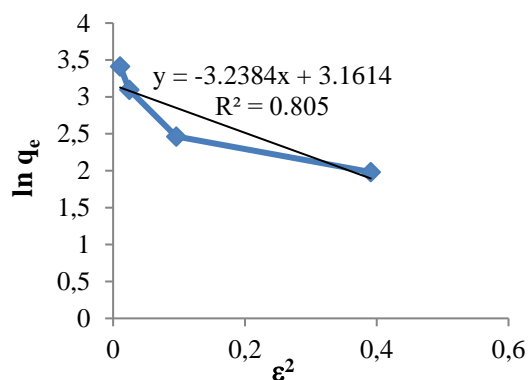


**Figure 13. The isotherm adsorption curves according to D-R models.**

Table 3 shows the common adsorbents generally applied for environmental treatment and MB in particular. The adsorption capacity of FGP - 3 in this study was lower than that of Chaukura (2017) and 2.4 times lower than that documented in Pham' study (2016). This study has a higher maximum

adsorption capacity than Jamal' study (2016) and Tran's study (2017). This shows the potential of FGP-3 adsorbent on MB removal. However, each adsorbent material will have different structural components, so the adsorption capacity will be different.

**Table 3. References of several adsorbents on methyl blue**

Adsorbents	pH	qmax (mg.g <sup>-1</sup> )	Authors
Bio-coal	12.0	33.0	(Chaukura et al., 2017)
Poly(3,4propylenedioxythiophen/MnO <sub>2</sub> composites)	7.0	13.9	(Jamal et al., 2016)
CS/Fe <sub>3</sub> O <sub>4</sub> /GO	10.5	30.1	(Hoang et al., 2017)
Fe <sub>3</sub> O <sub>4</sub> /GO	7.0	72.9	(Pham et al., 2016)
FGP-3	8.5	30.4	This study

#### 4. CONCLUSIONS

This study successfully used the waste battery materials to successfully synthesize GO materials using the Hummers method and successfully synthesized FGP-3 by the co-precipitation method resulting in high crystallinity, purity and stabilized the system by PVP surfactant. With an adsorption capacity of 30.4 mg.g<sup>-1</sup> at 12 h, the initial

concentration of 5 ppm, the weight of the material 50 mg and the pH 10.5, the highest efficiency was achieved at 91.8% for adsorbing MB. The results also showed that the MB adsorption process with FGP-3 was consistent with the second-order hypothetical model and was isothermal according to the Freundlich adsorption model. Moreover, physical adsorption was confirmed based on the Dubinin-Radushkevich model.

#### REFERENCES

- Brisebois, P., & Sijaj, M. (2020). Harvesting graphene oxide—years 1859 to 2019: a review of its structure, synthesis, properties and exfoliation, *Journal of Materials Chemistry C*, 8(5), 1517-1547.
- Chaukura, N., Murimba, E.C., & Gwenzi, W. (2017). Sorptive removal of methylene blue from simulated wastewater using biochars derived from pulp and paper sludge, *Environmental Technology & Innovation*, 8, 132-140.
- Chen, W., Li, S., Chen, C., & Yan, L. (2011). Self-assembly and embedding of nanoparticles by in situ reduced graphene for preparation of a 3D graphene/nanoparticle aerogel, *Advanced materials*, 23(47), 5679-5683.
- Cui, P., Lee, J., Hwang, E., & Lee, H. (2011). One-pot reduction of graphene oxide at subzero temperatures, *Chemical Communications*, 47(45), 12370-12372.
- Cui, Y., Wang, L., Gao, L., Hu, L., Yan, Q., Wei, & B. Du. (2015). EDTA functionalized magnetic graphene oxide for removal of Pb (II), Hg (II) and Cu (II) in water treatment: adsorption mechanism and separation property, *Chemical engineering journal*, 281, 1-10.
- Dreyer, D.R., Park, S., Bielawski, C.W., & Ruoff, R.S. (2010). The chemistry of graphene oxide, *Chemical Society Reviews*, 39(1), 228-240.
- El-Shafai, N. M., Abdelfatah, M. M., El-Khouly, M. E., El-Mehasseb, I. M., El-Shaer, A., Ramadan, M. S., Masoud, M. S., & El-Kemary, M. A. (2020). Magnetite nano-spherical quantum dots decorated graphene oxide nano sheet (GO/Fe<sub>3</sub>O<sub>4</sub>): electrochemical properties and applications for removal heavy metals, pesticide and solar cell. *Applied Surface Science*, 506, 144896.
- Feng, J., Mao, J., Wen, X., & Tu, M. (2011). Ultrasonic-assisted in situ synthesis and characterization of superparamagnetic Fe<sub>3</sub>O<sub>4</sub> nanoparticles, *Journal of Alloys and Compounds*, 509(37), 9093-9097.
- Guan, D., Fan, M., Wang, J., Zhang, Y., Liu, Q., & Jing, X. (2010). Synthesis and properties of magnetic solid superacid: SO<sub>4</sub><sup>2-</sup>/ZrO<sub>2</sub>-B<sub>2</sub>O<sub>3</sub>-Fe<sub>3</sub>O<sub>4</sub>, *Materials Chemistry and Physics*, 122(1), 278-283.
- Hummers, J.W.S., & Offeman, R.E. (1958). Preparation of graphitic oxide, *Journal of the American Chemical Society*, 80(6), 1339-1339.
- Ibrahim, I., Yunus, S., & Hashim, M. (2013). Relative performance of isopropylamine, pyrrole and pyridine as corrosion inhibitors for carbon steels in saline water at mildly elevated temperatures, *International Journal of Scientific & Engineering Research*, 4(2), 1-12.
- Iftekhar, S., Ramasamy, D.L., Srivastava, V., Asif, M.B., & Sillanpa. (2018). M. Understanding the factors affecting the adsorption of Lanthanum using different adsorbents: a critical review. *Chemosphere*, 204, 413-430.
- Jamal, R., Zhang, L., Wang, M., Zhao, Q., & Abdiryim, T. (2016). Synthesis of poly (3, 4-propylenedioxythiophene)/MnO<sub>2</sub> composites and

- their applications in the adsorptive removal of methylene blue, *Progress in Natural Science: Materials International*, 26(1), 32-40.
- Le, T.M.T., Pham, M.C., Tran, H.T, Hoang, M.N., Nguyen, H.H., & Mai, T.P. (2020). Fabrication of Magnetic Iron Oxide/Graphene Oxide Nanocomposites for Removal of Lead Ions from Water, *Chemical engineering*, 78.
- Lipson, H.S., & Stokes, A. (1942). The structure of graphite, Proceedings of the Royal Society of London. Series A. *Mathematical and Physical Sciences*, 181(984), 101-105.
- Luong, H.V.T., Nguyen, N.H., Khuu, G.H., Bui, Y.P., Thieu, Q.Q.V., Ngo, T.N.M., & Tran, T.B.Q. (2022). Preparation of Fe<sub>3</sub>O<sub>4</sub>/Hap nanoparticles from eggshells with highly adsorption capacity for methylene blue. *Can Tho University Journal of Science*, 14(2),18-27.
- Mashkoo, F., & Nasar, A. (2020). Magsorbents: Potential candidates in wastewater treatment technology—A review on the removal of methylene blue dye. *Journal of magnetism and magnetic materials*, 500, 166408.
- Morimoto, N., Kubo, T., & Nishina, Y. (2016). Tailoring the oxygen content of graphite and reduced graphene oxide for specific applications, *Scientific reports*, 6(1), 1-8.
- Munoz, Maria, P.J., & Elizabeth, C.M. (2018). *Prussian blue based batteries*. Springer International Publishing.
- Pham, T. L. H., Nguyen, T. H., Chung, D. G, Nguyen, T., Vu, N. P, Nguyen, V. Q., Tran, Q. H., Dinh, T. M. H., Ho, D. C., & Le, A. T. (2016). Facile synthesis and excellent adsorption property of GO-Fe<sub>3</sub>O<sub>4</sub> magnetic nanohybrids for removal of organic dyes. *Journal of Nanoscience and Nanotechnology*, 16(9), 9544-9556.
- Qin, L., Liang, S., Tang, Y., Tan, X., & Zhou, J. (2015). Influence of PVP on Solvothermal Synthesized Fe<sub>3</sub>O<sub>4</sub>/Graphene Composites as Anodes for Lithium-ion Batteries, *Electrochemistry*, 83(8), 619-623.
- Saini, R.D. (2017). Textile organic dyes: polluting effects and elimination methods from textile waste water, *Int J Chem Eng Res*, 9(1), 121-136.
- Stawinski, W., Węgrzyn, A., Danko, T., Freitas, O., Figueiredo, S., & Chmielarz, L. (2017). Acid-base treated vermiculite as high performance adsorbent: Insights into the mechanism of cationic dyes adsorption, regeneration, recyclability and stability studies, *Chemosphere*, 173, 107-115.
- Thema, F., Moloto, M., Dikio, E., Nyangiwe, N., Kotsedi, L., Maaza, M., & Khenfouch, M. (2013). Synthesis and characterization of graphene thin films by chemical reduction of exfoliated and intercalated graphite oxide, *Journal of Chemistry*.
- Tran, H.V., Bui, L.T., Dinh, T.T., Le, D.H., Huynh, C.D., & Trinh, A.X. (2017). Graphene oxide/Fe<sub>3</sub>O<sub>4</sub>/chitosan nanocomposite: a recoverable and recyclable adsorbent for organic dyes removal. Application to methylene blue. *Materials Research Express*, 4(3), 035701
- Tural, B., Ozkan, N., & Volkan, M. (2009). Preparation and characterization of polymer coated superparamagnetic magnetite nanoparticle agglomerates, *Journal of Physics and Chemistry of Solids*, 70(5), 860-866.
- Wang, Y., Xia, G., Wu, C., Sun, J., Song, & R., Huang, W. (2015). Carbohydr. Polym, 115, 686-693.
- Wei, M.P., Chai, H., Cao, Y.L., & Jia, D.Z. (2018). Sulfonated graphene oxide as an adsorbent for removal of Pb<sup>2+</sup> and methylene blue, *Journal of colloid and interface science*, 524, 297-305.
- Xiao, Z., Zhou, Q., H., Qin, Qiao, J., & Guan, X. (2016). The enhancing effect of weak magnetic field on degradation of Orange II by zero-valent iron, *Desalination and Water Treatment*, 57(4), 1659-1670.
- Yang, B., Wei, Y., Liu, Q., Luo, Y., Qiu, S., & Shi, Z. (2019). Polyvinylpyrrolidone functionalized magnetic graphene-based composites for highly efficient removal of lead from wastewater, *Colloids and Surfaces A: Physicochemical and Engineering Aspects*, 582, 123927.
- Zhang, P., Lo, I., O'Connor, D., Pehkonen, S., Cheng, H., & Hou, D. (2017). High efficiency removal of methylene blue using SDS surface-modified ZnFe<sub>2</sub>O<sub>4</sub> nanoparticles, *Journal of colloid and interface science*, 508, 39-48.